SAND2000-0453C

A FINITE ELEMENT MODEL OF FERROELECTRIC/FERROELASTIC POLYCRYSTALS

Stephen C. Hwang[1,*] and Robert M. McMeeking[2]

[1]Institut für Festkörperforschung, Forschungszentrum Jülich
D-52425, Jülich, Germany

[2]Department of Mechanical and Environmental Engineering
University of California, Santa Barbara, California 93106–5050, USA

RECEIVED
FEB 24 2000
OSTI

ABSTRACT

A finite element model of polarization switching in a polycrystalline ferroelectric/ferroelastic ceramic is developed. It is assumed that a crystallite switches if the reduction in potential energy of the polycrystal exceeds a critical energy barrier per unit volume of switching material. Each crystallite is represented by a finite element with the possible dipole directions assigned randomly subject to crystallographic constraints. The model accounts for both electric field induced (i.e. ferroelectric) switching and stress induced (i.e. ferroelastic) switching with piezoelectric interactions. Experimentally measured elastic, dielectric, and piezoelectric constants are used consistently, but different effective critical energy barriers are selected phenomenologically. Electric displacement *versus* electric field, strain *versus* electric field, stress *versus* strain, and stress *versus* electric displacement loops of a ceramic lead lanthanum zirconate titanate (PLZT) are modelled well below the Curie temperature.

Keywords: ferroelectricity, ferroelasticity, switching, finite element, piezoelectricity

1. INTRODUCTION

Renewed interest in ferroelectric memories as well as sensors, actuators and smart structures has brought resurgent research activity on this material since the mid 1970s augmenting prior work[1-8]. Recently, the development of nano-particle ceramics[9-11] and nano-thickness films[12,13], the characterization of switching mechanisms with sensitive surface scanning equipment[14,15] and measurements of the ferroelectric response at small field[16,17] enhance our understanding of ferroelectricity while bringing new technologies. However, only a modest amount of work has focused on mesoscopic modeling of the important nonlinear behavior of polycrystalline ceramics under electro-mechanical loads[18-26].

Ferroelectric switching occurs because of multiple equilibrium states allowed in the crystal structure (e.g. in tetragonal symmetry, a central ion can move into any one of six orthogonal off center sites due to the application of electric field, mechanical stress or both[27-28]). Theories for the switching between these equilibrium states involve potential energy reduction as a driving force[27,29,30] resisted by energy barriers between the various configurations (e.g. Landau-Ginzburg-Devonshire model). For a single crystal and a polycrystalline ceramic, the theories for switching encompass a modification of Avrami's nucleation and growth model based upon the kinetics of rate dependency[31-34]. Switching domains nucleating on the surface of a ceramic, expanding and eventually meeting other growing domains in a ceramic have been experimentally observed[1,3,35].

As regards our polarization switching model, the basic assumption is that a single ferroelectric crystallite in a polycrystalline ceramic, which is subjected to an electric field or a stress or both, undergoes a polarization change and a corresponding strain change if the resulting reduction in potential energy exceeds a critical value per unit volume of switching material. The critical value of energy reduction is assumed implicitly to be associated with barriers to switching which cause dissipation as domain walls sweep through the material. However, the crystallite is assumed to be a single domain, entirely switched into one of the available ferroelectric variants. The switch from one variant to another is thus taken to be instantaneous, so that rate effects are neglected. The crystallite's transformation causes a disruption of the local electric field and a strain mismatch at the crystallite boundary[22], contributing to the change of potential energy of the polycrystalline ceramic. In previous work, approximations to this contribution to the energy change of the system were obtained. The simplest approach was to neglect the interaction completely, leading to a Reuss approximation[18,19]. A mean field theory

*Current Address: Sandia National Laboratories, P.O. Box 5800, MS 0847, Albuquerque, NM 87185-0847, USA
Email: schwang@sandia.gov

based on approximating the interaction energy as that of a non-piezoelectric inclusion in a non-piezoelectric matrix has also been used[23]. Finite element models of polycrystals have also been developed, with each crystallite being represented by a single element. So far, these treatments have been applied only to purely ferroelectric[24] and purely ferroelastic[25] systems with electro-mechanical interactions neglected.

In the current work described below, the behavior of a polycrystalline ferroelectric/ferroelastic ceramic is developed with the dielectric, elastic and piezoelectric response accounted for. Yet the model is still a simplification. Each crystallite is modelled as a cube with each cube having the same size. Therefore, the distribution of grain shape and size is yet to be introduced. Furthermore, the progressive switching caused by a domain wall motion is neglected, although this effect has been handled elsewhere within the context of a mean field theory leading to a self-consistent treatment based on inclusion models[26].

The simulations using the finite element model are carried out with 256 cubic crystallites having initially random tetragonality and electrical polarization consistent with the tetragonality. The applied electrical or stress field is gradually increased and later reversed. The behavior is followed incrementally by permitting in each step the switching of the crystallites most favored in the sense of the driving force exceeding the critical barrier. At a given increment of the process the load is kept constant until all the energetically favorable domains switch and thereafter the load is changed. The parameters of the model are chosen from empirical constants of a lead lanthanum zirconate titanate (PLZT 8/65/35) ceramic[22].

In this paper, the spontaneous polarization is the switchable polarization of a crystallite and the spontaneous strain is the switchable strain of a crystallite; the remanent polarization is the switchable polarization of the polycrystalline ceramic and the remanent strain is the switchable strain of the polycrystalline ceramic; the remanent polarization and strain are the average over spontaneous values of all the crystallites in the ceramic.

2. GOVERNING EQUATIONS

The crystallites are bonded together perfectly at their boundaries with no extrinsic charge present anywhere within the ferroelectric ceramic. Thus, the electric displacement **D** satisfies[36]

$$\partial D_i / \partial x_i = 0 \tag{1}$$

along with the continuity condition

$$n_i \left[\left|D_i\right|\right] = 0 \tag{2}$$

across the crystallite boundaries where **x** is position, **n** is the outward unit normal to the boundary and the symbol $\left[\left|\ \right|\right]$ denotes a jump in the quantity contained within it, defined as the value outside the crystallite minus the value within. Without body force, mechanical equilibrium requires that

$$\partial \sigma_{ij} / \partial x_i = 0 \tag{3}$$

and

$$n_i \left[\left|\sigma_{ij}\right|\right] = 0 \tag{4}$$

across crystallite boundaries, where σ is the mechanical stress defined by a constitutive law for a given crystallite[19,27]

$$\sigma_{ij} = C_{ijkl}\left(e_{kl} - e^s_{kl}\right) - \gamma_{kij} E_k \tag{5}$$

where **C** is the elastic tensor and e^s is the spontaneous strain of the tetragonal unit cell measured from a cubic datum. The quantity **e** is the strain in a crystallite defined in terms of the displacement **u** in the usual manner,

$$e_{ij} = \left(\partial u_i / \partial x_j + \partial u_j / \partial x_i\right)/2 \tag{6}$$

and γ is the converse piezoelectric coefficient tensor[27] defined by

$$\gamma_{ijk} = d_{ilm} C_{lmjk} \tag{7}$$

DISCLAIMER

This report was prepared as an account of work sponsored by an agency of the United States Government. Neither the United States Government nor any agency thereof, nor any of their employees, make any warranty, express or implied, or assumes any legal liability or responsibility for the accuracy, completeness, or usefulness of any information, apparatus, product, or process disclosed, or represents that its use would not infringe privately owned rights. Reference herein to any specific commercial product, process, or service by trade name, trademark, manufacturer, or otherwise does not necessarily constitute or imply its endorsement, recommendation, or favoring by the United States Government or any agency thereof. The views and opinions of authors expressed herein do not necessarily state or reflect those of the United States Government or any agency thereof.

DISCLAIMER

Portions of this document may be illegible in electronic image products. Images are produced from the best available original document.

where **d** is the direct piezoelectric coefficient tensor. The electric field vector, E, is given by

$$E_i = -\partial \Phi / \partial x_i \tag{8}$$

where Φ is the potential. For the electric displacement **D**, each crystallite obeys[19,27]

$$D_i = \gamma_{ijk}\left(e_{jk} - e^s_{jk}\right) + \varepsilon_{ij} E_j + P^s_i \tag{9}$$

where ε is the tensor of dielectric permittivities at constant strain, and P^s is the spontaneous polarization of the crystallite with magnitude P_o.

3. ENERGY RELATIONSHIPS AND SWITCHING CRITERION

The potential energy of the polycrystalline ferroelectric/ferroelastic ceramic is given by[22,36,37]

$$U(\mathbf{u}, q, \mathbf{D}) = \frac{1}{2}\int_V \left[\sigma_{ij}\left(e_{ij} - e^s_{ij}\right) + E_i\left(D_i - P^s_i\right)\right] dV - \int_{S_T} T_i\, u_i\, dS - \int_{S_\Phi} q\, \Phi\, dS \tag{10}$$

where the first integral is the elastic, dielectric and piezoelectric energy stored in the material, the second is the potential energy of the traction **T** imposed on the part S_T of the boundary S, and the third is the potential energy of the electrical load Φ imposed on the part S_Φ of the boundary S. The potential energy is a functional of **u**, q and **D**, so that **E** and σ in eq. (10) should be considered as functions of **D** and **e**. Since q is taken to be zero on S - S_Φ and **u** to be zero on S - S_T, the potential energy can be rewritten as[22]

$$U(\mathbf{u}, q, \mathbf{D}) = \frac{1}{2}\int_V \left[\sigma_{ij}\left(e_{ij} - e^s_{ij}\right) + E_i\left(D_i - P^s_i\right)\right] dV - \int_S T_i\, u_i\, dS - \int_S q\, \Phi\, dS \tag{11}$$

A given crystallite switches when the reduction of the potential energy ΔU of the polycrystalline ceramic due to that switch is equal or larger than the energy barrier for the switch. Thus, the switching criterion is given by

$$\Delta U + V_c\, \Delta \psi_c \leq 0 \tag{12}$$

where $\Delta\psi_c$ is the energy barrier per unit volume of a crystallite which must be overcome upon switching and V_c is the volume of the crystallite which switches. The energy barrier to a 90° switch $\Delta\psi_c^{90}$ is taken to be either the same as or different from the barrier to a 180° switch $\Delta\psi_c^{180}$. Only the most favorably oriented crystallite is allowed to switch at any stage and only one is permitted to switch at any time. The most favorably oriented crystallite is defined to be the one for which the left hand side of eq. (12) is smallest.

The requirement that eqs. (1) to (9) must be satisfied after the switch will lead to changes in all the terms in U except **T** on S_T and Φ on S_Φ which are fixed. The spontaneous polarization of the crystallite changes from its old value P^s to a new value $P^s + \Delta P^s$ and the spontaneous strain changes from e^s to $e^s + \Delta e^s$. Due to the change of the spontaneous crystallite polarization and strain, the electric field in the polycrystal changes from its old value **E** to a new value **E** + ΔE, the strain becomes a new value **e** + Δe, the displacement on S_T becomes a new value **u** + Δ**u** and the charge on S_Φ becomes q + Δq. Consistent with the change of the crystallite tetragonality, the tensor of dielectric permittivities changes from its old value ε to a new value $\varepsilon + \Delta\varepsilon$; the elastic tensor becomes **C** + Δ**C**; and consistent with the change in spontaneous polarization, the converse piezoelectric coefficient tensor becomes $\gamma + \Delta\gamma$. The change of the energy in the system ΔU is thus given by

$$\begin{aligned}\Delta U = \frac{1}{2}\int_V \Big[&\sigma_{ij}\left(\Delta e_{ij} - \Delta e^s_{ij}\right) + E_i\left(\Delta D_i - \Delta P^s_i\right) + \Delta\sigma_{ij}\left(e_{ij} - e^s_{ij} + \Delta e_{ij} - \Delta e^s_{ij}\right) \\ &+ \Delta E_i\left(D_i - P^s_i + \Delta D_i - \Delta P^s_i\right)\Big] dV - \int_S T_i\, \Delta u_i\, dS - \int_S \Phi\, \Delta q\, dS\end{aligned} \tag{13}$$

The relationship between charge and electric displacement on S is

$$q = -n_i D_i \tag{14}$$

where **n** is the outward unit normal to the surface and **D** is taken to be zero outside of V. This latter assumption is justified by the relatively large effective dielectric constant for PLZT and the cubic shape of V. Virtual work then gives

$$\int_S \Phi\, \Delta q\, dS \;=\; \int_V E_i\, \Delta D_i\, dV \tag{15}$$

In addition, the virtual work relationship

$$\int_S T_i\, \Delta u_i\, dS \;=\; \int_V \sigma_{ij}\, \Delta e_{ij}\, dV \tag{16}$$

also prevails. Substitution of these results into eq. (13) leads to

$$\begin{aligned}\Delta U \;=\; & -\int_V \left(\sigma_{ij}\, \Delta e^s_{ij} + E_i\, \Delta P^s_i\right) dV - \frac{1}{2}\int_V \Big[\sigma_{ij}\left(\Delta e_{ij} - \Delta e^s_{ij}\right) + E_i\left(\Delta D_i - \Delta P^s_i\right) \\ & - \Delta\sigma_{ij}\left(e_{ij} - e^s_{ij} + \Delta e_{ij} - \Delta e^s_{ij}\right) - \Delta E_i\left(D_i - P^s_i + \Delta D_i - \Delta P^s_i\right)\Big] dV\end{aligned} \tag{17}$$

A further application of virtual work leads to

$$\int_V \Delta\sigma_{ij}\, \Delta e_{ij}\, dV \;=\; \int_S \Delta T_i\, \Delta u_i\, dS. \tag{18}$$

The boundary conditions applied on S ensure that the right hand side of eq. (18) is zero. For convenience, we can therefore write

$$\begin{aligned}\Delta U \;&=\; \Delta U - \int_V \Delta\sigma_{ij}\, \Delta e_{ij}\, dV \\ &=\; -\int_V \left(\sigma_{ij}\, \Delta e^s_{ij} + E_i\, \Delta P^s_i\right) dV - \frac{1}{2}\int_V \Big[\sigma_{ij}\left(\Delta e_{ij} - \Delta e^s_{ij}\right) + E_i\left(\Delta D_i - \Delta P^s_i\right) \\ & \quad - \Delta\sigma_{ij}\left(e_{ij} - e^s_{ij} - \Delta e_{ij} - \Delta e^s_{ij}\right) - \Delta E_i\left(D_i - P^s_i + \Delta D_i - \Delta P^s_i\right)\Big] dV\end{aligned} \tag{19}$$

The stress increment is given by

$$\Delta\sigma_{kl} \;=\; C_{ijkl}\left(\Delta e_{ij} - \Delta e^s_{ij}\right) + \Delta C_{ijkl}\left(e_{ij} - e^s_{ij} + \Delta e_{ij} - \Delta e^s_{ij}\right) - \gamma_{ikl}\Delta E_i - \Delta\gamma_{ikl}\left(E_i + \Delta E_i\right) \tag{20}$$

and the electric displacement increment by

$$\Delta D_i \;=\; \gamma_{ijk}\left(\Delta e_{jk} - \Delta e^s_{jk}\right) + \Delta\gamma_{ijk}\left(e_{jk} - e^s_{jk} + \Delta e_{jk} - \Delta e^s_{jk}\right) + \varepsilon_{ij}\,\Delta E_j + \Delta\varepsilon_{ij}\left(E_j + \Delta E_j\right) + \Delta P^s_i \tag{21}$$

Substitution of these into eq. (19) along with eq. (5) and (9) into its second integral gives

$$\begin{aligned}\Delta U \;=\; & -\int_V \left(\Delta e^s_{ij}\,\sigma_{ij} + \Delta P^s_i\, E_i\right) dV + \frac{1}{2}\int_V \Delta e^s_{ij}\, C_{ijkl}\, \Delta e^s_{kl}\, dV - \frac{1}{2}\int_V \Delta e_{ij}\left(C_{ijkl} + \Delta C_{ijkl}\right)\Delta e_{kl}\, dV \\ & + \frac{1}{2}\int_V \left(e_{ij} - e^s_{ij} - \Delta e^s_{ij}\right)\Delta C_{ijkl}\left(e_{kl} - e^s_{kl} - \Delta e^s_{kl}\right) dV + \int_V \Delta E_i\left(\gamma_{ijk} + \Delta\gamma_{ijk}\right)\Delta e_{jk}\, dV \\ & - \int_V E_i\,\Delta\gamma_{ijk}\left(e_{jk} - e^s_{jk} - \Delta e^s_{jk}\right) dV + \frac{1}{2}\int_V \Delta E_i\left(\varepsilon_{ij} + \Delta\varepsilon_{ij}\right)\Delta E_j\, dV - \frac{1}{2}\int_V E_i\,\Delta\varepsilon_{ij}\, E_j\, dV\end{aligned} \tag{22}$$

4. FINITE ELEMENT METHOD

The finite element equations for solving the problem can be developed from the principle of the virtual work[38]

$$\int_V \left(\delta e_{ij}\,\sigma_{ij} - \delta E_i\, D_i\right) dV \;=\; \int_S \left(\delta u_i\, T_i - \delta\Phi\, q\right) dS \tag{23}$$

where $\delta(\,)$ indicates a virtual variation. The mechanical boundary conditions are

$$\begin{aligned} n_i\,\sigma_{ij} \;&=\; T^o_j \qquad \text{on } S_T, \\ u_i \;&=\; 0 \qquad \text{on } S_u \end{aligned} \tag{24}$$

where T^o is the prescribed traction given on S_T and $S_u + S_T = S$. As noted previously, it is assumed that the electrostatic energy in regions external to V can be neglected because of the high dielectric permittivity of the polycrystal compared to that of air. As a result, **D** is neglected outside V and $n_i\left[\left|D_i\right|\right] = -\,n_i\, D_i$ on the surface S. Thus, the electrical boundary conditions are

$$\begin{aligned} n_i D_i &= 0 \qquad \text{on } S_q, \\ \Phi &= \Phi^o \qquad \text{on } S_\Phi \end{aligned} \tag{25}$$

where Φ^o is the prescribed electric potential on S_Φ and $S_q + S_\Phi = S$. In a matrix notation, the displacement components of u and the potential Φ can be written in terms of finite element interpolations as

$$\begin{aligned} \begin{Bmatrix} u_1 \\ u_2 \\ u_3 \end{Bmatrix} &= [N_u]\{\omega_N\}, \\ \Phi &= [N_\Phi]\{\omega_N\} \end{aligned} \tag{26}$$

where the matrix $[N_u]$ contains interpolation functions of the displacement and $[N_\Phi]$ contains interpolation functions of the electric potential. The vector $\{\omega_N\}$ contains the displacements and the potentials for all the nodal points in the finite element mesh[39]. The strain for each element in {e} and the electric field for each element in {E} are given in column vectors as

$$\begin{aligned} \{e_{11}\ e_{22}\ e_{33}\ 2e_{23}\ 2e_{13}\ 2e_{12}\}^T &= \{e\} = [B_e]\{\omega_N\}, \\ \{E_1\ E_2\ E_3\}^T &= \{E\} = [B_E]\{\omega_N\} \end{aligned} \tag{27}$$

where the interpolation matrices $[B_e]$ and $[B_E]$ result from differentiations of $[N_u]$ and of $[N_\Phi]$, respectively. In a discretized form, eq. (23) becomes after elimination of virtual variations of $\{\omega_N\}$

$$\int_V \left([B_e]^T \{\sigma\} - [B_E]^T \{D\} \right) dV = \int_{S_T} [N_u]^T \{T\}^o \, dS \tag{28}$$

where $\{\sigma\}$ is a column vector containing stress components in the same order as in {e}, {D} is a column vector containing electric displacement components in the same order as in {E}, {T} is $\{T_1\ T_2\ T_3\}^T$ and the superscript o indicates prescribed values. The surface integral over S_q in eq (28) is absent because the charge is prescribed to be zero there.

Use of the constitutive laws eqs. (5) and (9) then give the finite element equations

$$[K]\{\omega_N\} = \{F\} + \{F^s\} \tag{29}$$

where [K] is the stiffness matrix, {F} is the nodal load due to the tractions T^o on S_T and $\{F^s\}$ is the additional nodal load due to the spontaneous polarization and spontaneous strain. The stiffness matrix [K] and column vectors {F} and $\{F^s\}$ are given as

$$\begin{aligned} [K] &= \int_V \left([B_e]^T [C][B_e] - [B_e]^T [\gamma][B_E] - [B_E]^T [\gamma]^T [B_e] - [B_E]^T [\varepsilon][B_E] \right) dV \\ \{F\} &= \int_{S_T} [N_u]^T \{T\} \, dS \\ \{F^s\} &= \int_V \left([B_e]^T [C]\{e^s\} - [B_E]^T [\gamma]^T \{e^s\} + [B_E]^T \{P^s\} \right) dV \end{aligned} \tag{30}$$

where the matrix [C] contains the elastic constants, the matrix $[\gamma]$ contains the converse piezoelectric coefficients, and the matrix $[\varepsilon]$ contains the dielectric permittivities such that

$$\begin{aligned} \{\sigma\} &= [C]\left(\{e\} - \{e^s\} \right) - [\gamma]\{E\}, \\ \{D\} &= [\gamma]^T \left(\{e\} - \{e^s\} \right) + [\varepsilon]\{E\} + \{P^s\}. \end{aligned} \tag{31}$$

which is equivalent to eqs. (5) and (9). The matrices [C], $[\gamma]$ and $[\varepsilon]$ are the same in crystallographic axis with the third direction aligned with the spontaneous polarization. However, when rotated to global coordinates, the matrices will vary from element to element due to the orthogonal transformation.

In a discretized form, the reduction of the potential energy due to switching from eq. (22) is

$$\Delta U = -\int_V \left(\{\Delta e^s\}^T \{\sigma\} + \{\Delta P^s\}^T \{E\} \right) dV + \frac{1}{2} \int_V \{\Delta e^s\}^T [C] \{\Delta e^s\} dV$$
$$+ \frac{1}{2} \int_V \left(\{e^s\}^T + \{\Delta e^s\}^T - \{e\}^T \right) [\Delta C] \left(\{e^s\} + \{\Delta e^s\} - \{e\} \right) dV \tag{32}$$
$$+ \int_V [E]^T [\Delta \gamma]^T \left(\{e^s\} + \{\Delta e^s\} - \{e\} \right) dV - \frac{1}{2} \int_V \{E\}^T [\Delta \varepsilon] \{E\} dV - \frac{1}{2} \{\Delta \omega_N\}^T \left([K] + [\Delta K] \right) \{\Delta \omega_N\}$$

The increments of nodal displacements $\{\Delta\omega_N\}$ due to switching must satisfy the finite element equation

$$[K]\{\Delta \omega_N\} + [\Delta K]\left(\{\omega_N\} + \{\Delta \omega_N\}\right) = \{\Delta F^s\} \tag{33}$$

which is an incremental form of eq. (29). Since the prescribed tractions are held fixed during a switch and the prescribed charges are set to be zero on S_q, only the nodal load increments due to the change of the spontaneous polarization and strain appear on the right hand side of eq. (33). The column vector of this nodal load increments is given from eq. (30)

$$\{\Delta F^s\} = \int_V \Big\{ [B_e]^T \left[[C]\{\Delta e^s\} + [\Delta C]\left(\{e^s\} + \{\Delta e^s\}\right) \right]$$
$$- [B_E]^T \left[[\gamma]^T \{\Delta e^s\} + [\Delta \gamma]^T \left(\{e^s\} + \{\Delta e^s\} \right) \right] + [B_E]^T \{\Delta P^s\} \Big\} dV \tag{34}$$

and the stiffness matrix increment is also given from eq. (30) as

$$[\Delta K] = \int_V \left([B_e]^T [\Delta C] [B_e] - [B_e]^T [\Delta \gamma] [B_E] - [B_E]^T [\Delta \gamma]^T [B_e] - [B_E]^T [\Delta \varepsilon] [B_E] \right) dV \tag{35}$$

Solving for $[\Delta\omega_N]$ in eq. (33) gives

$$\{\Delta \omega_N\} = \left([K] + [\Delta K] \right)^{-1} \left(\{\Delta F^s\} - [\Delta K]\{\omega_N\} \right). \tag{36}$$

Thus, the reduction of the potential energy in eq. (32) becomes

$$\Delta U = -\int_V \Big[\{\Delta e^s\}^T \{\sigma\} + \{\Delta P^s\}^T \{E\} - \frac{1}{2} \{\Delta e^s\}^T [C] \{\Delta e^s\}$$
$$- \frac{1}{2} \left(\{e^s\}^T + \{\Delta e^s\}^T - \{e\}^T \right) [\Delta C] \left(\{e^s\} + \{\Delta e^s\} - \{e\} \right) - \{E\}^T [\Delta \gamma]^T \left(\{e^s\} + \{\Delta e^s\} - \{e\} \right) \tag{37}$$
$$+ \frac{1}{2} \{E\}^T [\Delta \varepsilon] \{E\} \Big] dV - \frac{1}{2} \left(\{\Delta F^s\} - [\Delta K]\{\omega_N\} \right)^T \left([K] + [\Delta K] \right)^{-1} \left(\{\Delta F^s\} - [\Delta K]\{\omega_N\} \right)$$

5. NUMERICAL SIMULATION

The model for ferroelectric behavior is implemented in a finite element mesh of a few hundred crystallites. The mesh consists of cubic elements of equal size arranged in a cube as depicted for 8 elements in Fig. 1. Each finite element represents one crystallite; each element has eight nodes with a node at each corner[39]. Parallel to the coordinate direction, the elements use a linear interpolation of each displacement component and the potential, so that there is a trilinear dependence on position. The strain, stress, electric field, and electric displacement in each element are evaluated at the centroid and the stiffness in eq. (30) is computed by 1 point numerical integration[39]. A random number generator is used to create the principal axes of the initial tetragonal unit cell of each crystallite. The magnitude of the spontaneous strain of a crystallite parallel to the c-axis of the unit cell is

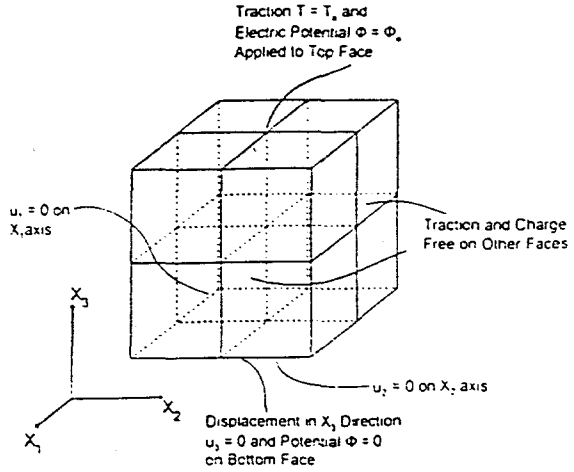

FIG. 1. Schematic diagram of the cubic mesh of 8 elements. Each cubic element represents one crystallite and has its own principal crystallographic directions.

$e_o = \frac{c - a_o}{a_o}$. The strain perpendicular to the c-axis is $-\frac{1}{2} e_o = \frac{a - a_o}{a_o}$, where a_o is the lattice parameter of a cubic cell having the same volume as the tetragonal cell. A spontaneous polarization of magnitude P_o is assigned randomly to the positive or negative direction parallel to the c-axis of the unit cell. The spontaneous polarizations along the a-axes are zero. The components of the spontaneous strain and polarization of each crystallite are calculated in a fixed Cartesian coordinate system common to the ceramic. These components will be referred to throughout the discussion below.

The dielectric permittivity, piezoelectric coefficient and elasticity tensors in general are anisotropic with the polar axis determining the symmetries. However, there are insufficient experimental data to determine values other than that parallel to the poled axis of 8/65/35 PLZT single crystallite. Thus, the permittivity is taken to be isotropic

$$\varepsilon_{ij} = \varepsilon \delta_{ij} \tag{38}$$

where ε is the dielectric permittivity and the elasticity matrix is also taken to be isotropic

$$C_{ijkl} = \frac{Y \nu}{(1+\nu)(1-2\nu)} \delta_{ij} \delta_{kl} - \frac{Y}{2(1+\nu)} \left(\delta_{ik} \delta_{jl} + \delta_{il} \delta_{jk} \right) \tag{39}$$

where ν is Poisson's ratio and Y is Young's modulus. The values for ε, ν and Y are chosen to match the experimental data measured from uniaxial poling and stressing experiments on the polycrystalline ceramic. With these assumptions, the dielectric permittivity and the elasticity of the polycrystalline ceramic will be isotropic even when it has a net polarization. The direct piezoelectric coefficient tensor for each crystallite, when referred to the coordinate system in which the positive x_3-axis is parallel to the positive polarization direction, has the positive valued component d_{333}[27]. The other components of d which are nonzero are assumed to be

$$d_{311} = d_{322} = -\frac{1}{2} d_{333} \tag{40}$$

Contribution of the shear components of d to the macroscopic average piezoelectric behavior is significant, but none of the shear components are provided by the PLZT experiments[19]. With the isotropic elastic constant C and the direct piezoelectric coefficient tensor d, the nonzero components of the converse piezoelectric coefficient tensor g in eq. (7) are stated as

$$\begin{aligned} \gamma_{333} &= \frac{d_{333} Y}{(1+\nu)} \\ \gamma_{311} &= \gamma_{322} = -\frac{1}{2} \gamma_{333} \end{aligned} \tag{41}$$

The macroscopic strain of the aggregate is computed as the volume average of the strain in the crystallites and the macroscopic polarization is the volume average of the spontaneous polarization in the crystallites. Since each crystallite has the same volume V_c, the volume average can be computed as a simple arithmetic average of the strain and polarization components over all crystallites. Thus, the initial remanent strain and polarization of the polycrystal is zero (or nearly zero because the finite number of crystallites involved in a given simulation can have a nonzero average from the random number generation). Similarly, the average linear contributions to the strain **e** and the electric displacement **D** are zero initially since the imposed traction and potential are zero initially.

The boundary conditions in eq. (24) are imposed such that the displacement u_3 is fixed at zero for all nodal points on the bottom surface of the cubic mesh as shown in Fig. 1 where the X_3-axis is considered to be vertical and X_1 and X_2 define the horizontal plane. The displacement u_1 is fixed at zero for all points along the lower left edge of the cube and u_2 is zero along the lower front edge. All these nodal points where the displacement is fixed at zero compose S_u. As shown in Fig. 1, the traction is imposed on the top surface of the cube as a uniform value $T_3 = T^o$ with T_1 and T_2 equal to zero everywhere except on S_u. In addition, the boundary conditions in eq. (25) are imposed by fixing the electric potential Φ at zero on the bottom surface of the cube; the charge q is fixed at zero for all points on the side faces of the cube; and the potential is imposed on the top surface of the cube as a uniform value which is consistent with a uniform electric field.

A crystallite is assumed to switch when the reduction of potential energy of the system due to that switch is equal to a critical value, which can be considered to be equal to the energy barrier which must be overcome to achieve the switch. The switching criterion eq. (12) is modified in the form:

$$\{\Delta e^s\}^T\{\sigma\} + \{\Delta P^s\}^T\{E\} - \frac{1}{2}\{\Delta e^s\}^T[C]\{\Delta e^s\} - [E]^T[\Delta\gamma]^T\left(\{e^s\} + \{\Delta e^s\} - \{e\}\right)$$
$$+ \frac{1}{2V_e}\left(\{\Delta F^s\} - [\Delta K]\{\omega_N\}\right)^T([K] + [\Delta K])^{-1}\left(\{\Delta F^s\} - [\Delta K]\{\omega_N\}\right) \geq 2E_o P_o \qquad (42)$$

where V_e is the volume of an element and the term $\Delta\psi_e$ in eq. (12) is replaced by its value $2E_o P_o$ with E_o the magnitude of an effective coercive field. The parameter E_o is the coercive field parallel to the polarization direction for 180° switching in an isolated single crystallite. The switching criterion is evaluated at the centroid of an element with centroidal values of the strain, stress, spontaneous strain, electric field, and spontaneous polarization taken to represent the element as a whole. Since switching is considered for one element at a time, the first 4 terms on the left hand side of eq. (42) are computed only for the element under consideration for switching. The last term on the left hand side of eq.(42) accounts for the elastic, dielectric, and piezoelectric interaction energy of all the crystallites.

A new inverse stiffness matrix $[K]^{-1}$ is evaluated and stored after every switch because [K] changes to a new value due to the presence of anisotropic piezoelectric coefficients which lead to the increments $[\Delta\gamma]$. With the Sherman-Morrison formula[40], the new inverse $[K]^{-1}$ is then used to calculate $([K]-[\Delta K])^{-1}$ for all possible switches (i.e. five possible ferroelectric switches for tetragonal symmetry) for each crystallite. Note that $[K]^{-1}$ and $([K]-[\Delta K])^{-1}$ must be conditioned, as must be [K] in eq. (29) and ([K]-[ΔK]) in eq. (33), to account for displacement boundary conditions imposed on S_u and for potential boundary conditions on S_Φ. This is a trivial step since all boundary conditions on S_u and S_Φ involve zero value except for the prescribed uniform potential value on the top surface.

Since only one crystallite element is considered for switching at a time, the value of the left hand side of eq. (42) for the switch of one element of volume V_e can be identified. If the condition in eq. (42) is met, a switch is permissible. All possible switches in the aggregate (including the possible switches to different polarization in each element) are considered and the most favorable possibility is identified and accepted. The most favorable switch is that which causes the greatest reduction in potential energy; i.e. the switch for which the left hand side of eq. (42) most exceeds the right hand side. After the switch has been made, a new stiffness matrix [K] in eq. (29) is computed by rotating the converse piezoelectric tensor [γ] of the switched crystallite. A new nodal load $\{F^s\}$ is computed by reassembling the spontaneous strains and polarizations of all the crystallites in the finite element mesh. Solution of eq. (29) with the new [K] and $\{F^s\}$ gives new nodal values of i.e. $\{\omega_N\}$; the new nodal values then provide the new strain tensor $\{e\}$, stress tensor $\{\sigma\}$, and electric field vector $\{E\}$ in each element; the new [K] and its inverse $[K]^{-1}$ are then used to evaluate $([K]-[\Delta K])^{-1}$ for every possible switch for each element. Note that the exact inverse $([K]-[\Delta K])^{-1}$ for every possible switch is obtained from the Sherman-Morrison formula[40], easing the computational burden. With $\{\omega_N\}$, $\{\sigma\}$, $\{E\}$, and $([K]-[\Delta K])^{-1}$ updated, another switch associated with the greatest value of the left hand side of eq. (42) is then considered without changing the imposed traction or potential. This process is repeated until no more elements will switch. The traction or potential is then incremented and eq. (42) is used to select further switches. The increments of the traction or potential are estimated with the intention that only one crystallite switches at any given stage. However, once a crystallite switches, many other neighboring crystallites tend to follow suit.

6. RESULTS

All the calculations presented in this paper are done with an identical random set of 256 crystallites. Each crystallite is represented by an eight-node cubic finite element having a node at each corner in a 8 x 8 x 4 (i.e. 4 vertical layers of an 8 x 8 planar mesh) rectangular array with its rectangular edges parallel to the Cartesian coordinate axes common to the ceramic. The parameters used are experimentally determined values for 8/65/35 PLZT ceramic, Y = 68 GPa, ε = 0.05625 μF/m, d_{333} = 1.188 x 10^{-9} m/V, and υ = 0.48. The value e_o = 0.00277 is chosen in attempts to match the remanent strain and P_o = 0.34 C/m^2 chosen to match the remanent polarization of the experimental data after the sample was poled numerically and the field was removed.

Two sets of simulations are presented. For the first set of simulations, the effective critical field for 90° switching E_o^{90} is taken to be equal to the critical field for 180° switching E_o^{180} and both represented by E_o in eq. (42) which is selected to be 0.36 MV/m. The value of 0.36 MV/m is the measured coercive field for a PLZT ceramic. For the other set of simulations, the effective critical field for 90° switching E_o^{90} is set to be 0.10 MV/m and the critical field for 180° switching E_o^{180} is 1.0 MV/m. These critical values are used instead of E_o in eq. (42) for the relevant switch. Note that 0.10 MV/m is the effective critical field giving the best fit to the experimental electric displacement *versus* electric field hysteresis loop when only electric field induced (i.e. ferroelectric) switching is accounted for and strain and mechanical stress are neglected[24].

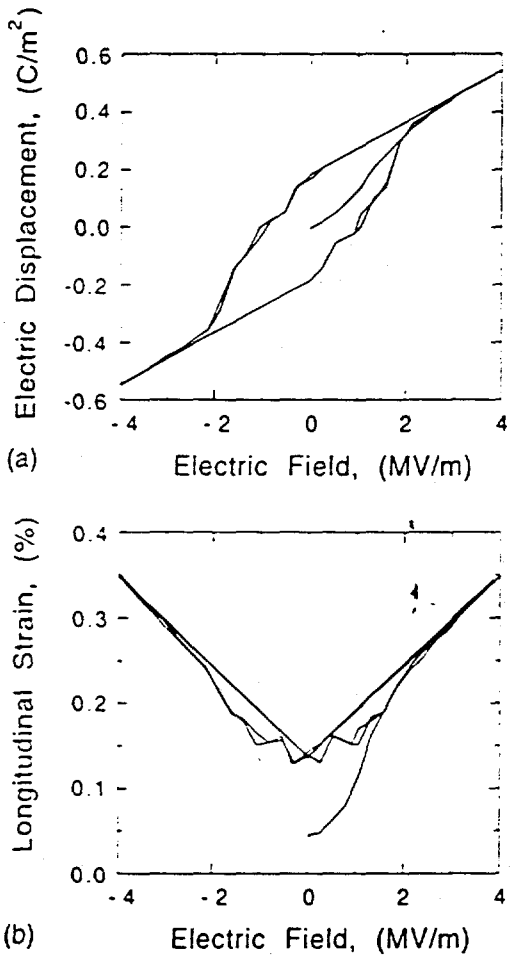

FIG. 2. Simulated 8/65/35 PLZT hysteresis loops with no applied stress and with the effective critical field of switching E_0 = 0.36 MV/m. (a) Electric displacement *versus* electric field. (b) Axial strain *versus* electric field.

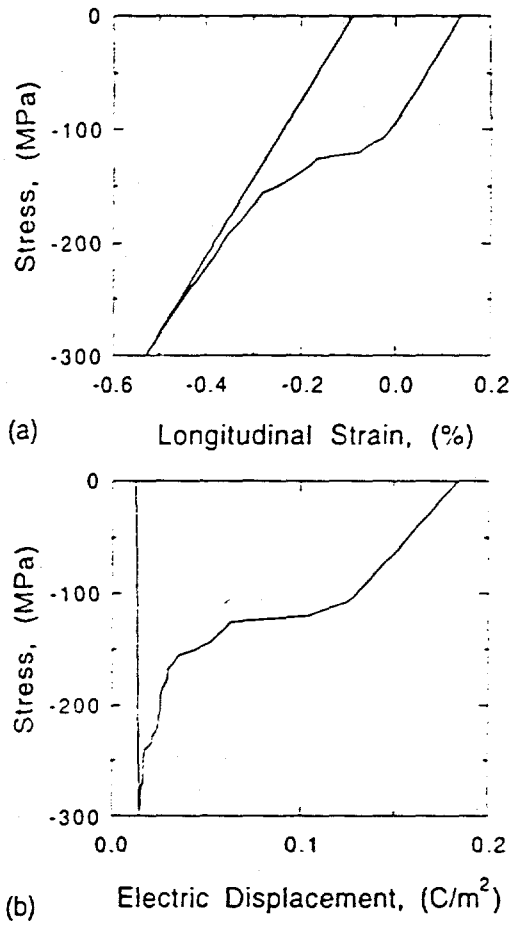

FIG. 3. Simulated 8/65/35 PLZT stress *versus* strain and stress *versus* electric displacement curves for a poled ceramic with no applied field and with the effective critical field of switching E_0 = 0.36 MV/m. (a) Axial stress *versus* axial strain. (b) Axial stress *versus* electric displacement.

6.1. Simulations with E_0 = 0.36 MV/m

Fig. 2(a) shows the simulated electric displacement *versus* electric field loop and 2(b) shows the corresponding longitudinal strain *versus* electric field butterfly loop with E_0 equal to 0.36 MV/m. The average remanent polarization and strain are zero initially because the elements have random spontaneous polarizations. This random state is then subjected to the switching criterion of eq. (42) without any applied electric field or stress and some switching occurs: the switching process in the absence of the applied load is called 'annealing'. When the annealing is completed, the macroscopic remanent polarization and strain are recorded. It can be seen in Fig. 2(b) that annealing leads to a small non-zero remanent strain.

As the applied potential is increased from zero in Fig. 2(a), the electric displacement increases linearly up to a field of 0.3 MV/m, rises nonlinearly from 0.3 MV/m to 1.3 MV/m, and thereafter increases nearly linearly, but the slope eventually decreases to the linear dielectric response at 3.0 MV/m. These nonlinearities in the initial curve occur only when a switch induces a large mechanical strain and internal stress[41]. If the mechanical strain is small, the electric displacement initially increases proportional to the square of the field until close to the coercive field (conforming to the Rayleigh law[16,42]), then rises rapidly beyond the coercive field, and eventually reaches the saturated polarization. Along the initial curve in Fig. 2(a), about an equal number of 90° and 180° switches occur. As the field reaches its maximum value of 4.0 MV/m, the spontaneous polarizations of some elements are aligned as much as possible with the applied electric field (i.e. poled), but many other elements are yet to be poled. At the maximum field, the remanent polarization—linear dielectric *contribution*

subtracted from the electric displacement—reaches only 87% of its potential value because strong mechanical constraints restrict poling of the ceramic by discouraging 90° switching[19,41]. Limited 90° switching occurs with nearly linear response of the electric displacement if the electric field is increased further beyond 4 MV/m, but the complete poling of the ceramic can be induced only with an extremely large electric field. As the field is lowered from 4 MV/m, the electric displacement reduces linearly until near zero field. Thereafter, significant reverse poling takes place at -0.30 MV/m, but the overall reverse response is gradual and incremental.

Fig. 2(b) shows the strain *versus* electric field butterfly loop corresponding to the electric displacement *versus* electric field hysteresis loop shown in Fig. 2(a). As the electric field is increased from zero initially, the strain initially increases slightly due to the linear piezoelectric response and then stays at a constant level until 0.3 MV/m. As the field is increased beyond 0.3 MV/m, the strain rises again until the field reaches 1.3 MV/m. Thereafter, the slope reduces gradually down to the linear piezoelectric response at a field level of about 4.0 MV/m. At the maximum field, the remanent strain reaches 89% of its potential value. The applied field is then decreased and the strain decreases mainly due to linear piezoelectric response until the strain reaches its minimum when the field is -0.3 MV/m. The strain then rises non-monotonically to reach near to saturation after repolarization. This non-monotonic response is never observed in measured strain *versus* electric field loops of PLZT ceramic.

The step-wise switching process shown in Figs. 2(a) and (b) is the result of the large constraints induced by the elastic, dielectric, and piezoelectric interaction energy resisting a switch: the barrier to switching is thus the sum of the constraints and the effective critical field for crystallite switching E_o. In a simulation, the switch of an element may induce a localized internal stress change in a crystallite as large as 300 MPa and an electric field change as large as 2 MV/m. These large fields can cause the follow-up switching of nearest neighbors. The follow-up switches, however, do not propagate through the ceramic: the propagation of the switching (i.e. the autocatalytic process) is short lived because of crystallites not yielding either mechanically or electrically due to the large constraints induced by the interaction energy. After the propagation of switching ends, a substantially higher applied field is required to initiate any further switching. The intermittent, step-wise switching in the simulation is an inaccurate description of the real ferroelectric switching in which the propagation of switching is widespread throughout the polycrystal as predicted by a modified Avrami nucleation and growth model[31-34]. During reverse poling, most crystallites undergo one direct 180° switches, but some undergo two consecutive 90° switches: 180° switching is favored over 90° switching since no strain change is involved in 180° switching. It is to be noted an equal critical field for 90° and 180° switching is used for this simulation. When a 90° switch occurs, the switched crystallite usually undergoes a second 90° switch immediately to reduce the mechanical strain created by its first 90° switch. Note that the strain curve in Fig. 2(b) is smoother during reverse poling in the range -1.5 to -4.0 MV/m than the curve for electric displacement in Fig. 2(a). This gradual electrical poling indicates that 180° switch has dominated and some crystallites are yet to be poled by further 90° switches.

Fig. 3 shows the axial stress *versus* longitudinal strain and the corresponding axial stress *versus* electric displacement when E_o = 0.36 MV/m. After poling the ceramic to a remanent polarization of 0.18 C/m^2 and a remanent strain of 0.14% as shown in Fig. 2, the field is reduced to zero. A compressive stress is then applied. The interaction energy (or mechanical and electric constraints), accounted for in the last term on the left hand side of the switching criterion in eq. (42), causes the stress at which switching first occurs to be 120 MPa of which more than half is induced by the constraints. (For ferroelastic switching, the right hand term $2E_oP_o$ in eq. (42) can be replaced by $1.5\sigma_o e_o$ where the effective critical stress for switching is σ_o The value corresponding to E_o = 0.36 MV/m is σ_o = 59 MPa.) Beyond the stress of 120 MPa, switching occurs gradually in Figs. 3(a) and (b) and stress induced depolarization is induced. When the compressive stress is reduced after the peak, almost no nonlinear strain and polarization change occurs.

6.2. Simulations with E_o^{90} = 0.10 MV/m and E_o^{180} =1.0 MV/m

Fig. 4 shows the electric displacement *versus* electric field hysteresis loop and the corresponding strain *versus* electric field butterfly loop when the critical field for 90° switching E_o^{90} = 0.10 MV/m and the critical field for 180° switching E_o^{180} = 1.0 MV/m. The low E_o^{90} suppresses 180° switching completely. The electric displacement loop in Fig. 4(a) has a low remanent polarization of 0.15 C/m^2 after a field is applied up to 4 MV/m and removed. In addition, the switching is gradual throughout the increase of the field. Upon reversal of the field, linear response ensues until the field is zero and then reverse switching sets in again. Cycling of the electric field then gives a repeatable loop. Fig. 4(b) shows the corresponding strain *versus* electric field loop. The strain initially rises approximately to 0.13% at zero field during annealing. (A simulation with a different random set of crystallites results in a different initial strain, but the strain value after annealing is usually above

0.1%.) The rise in strain during annealing is the effect of the crystallites aligning their c-axes to reduce elastic mismatches and thus to lower the global internal elastic energy. The strain loop also has shallow rounded tails instead of the typical deep narrow ones observed in the measured butterfly loops[19]. During polarization reversal, combinations of 90° switches occur. After undergoing a first 90° switch, many elements instantaneously undergo their second 90° switches to reduce their internal energy. As a result, there are only modest changes in the remanent strain in the switching process, as can be seen in Fig. 4(b).

Fig. 5 shows the axial stress *versus* longitudinal strain and the corresponding axial stress *versus* electric displacement, with E_o^{90} = 0.10 MV/m and E_o^{180} = 1.0 MV/m, induced by a compressive stress applied to the aggregate after cycling as shown in Fig. 4. The mechanical and electrical constraints of interaction among the crystallites enlarge the simulated coercive stress to approximately 100 MPa whereas the effective critical stress of switching, σ_o, corresponding to E_o^{90} = 0.10 MV/m (i.e. 90° switching is induced under stress) is only 16 MPa. The simulation shows that significant depolarization occurs at low compressive stress as observed in experiments[19]. The pattern of switching observed at higher compressive stress (i.e. the erratic depolarization curve in Fig. 5(b)) is a consequence of some elements undergoing reverse switching, following switches of a neighboring element. This is due to the low σ_o being easily overcome by constraint interaction effects and large mechanical and electrical depolarization stresses then favor the reverse switching.

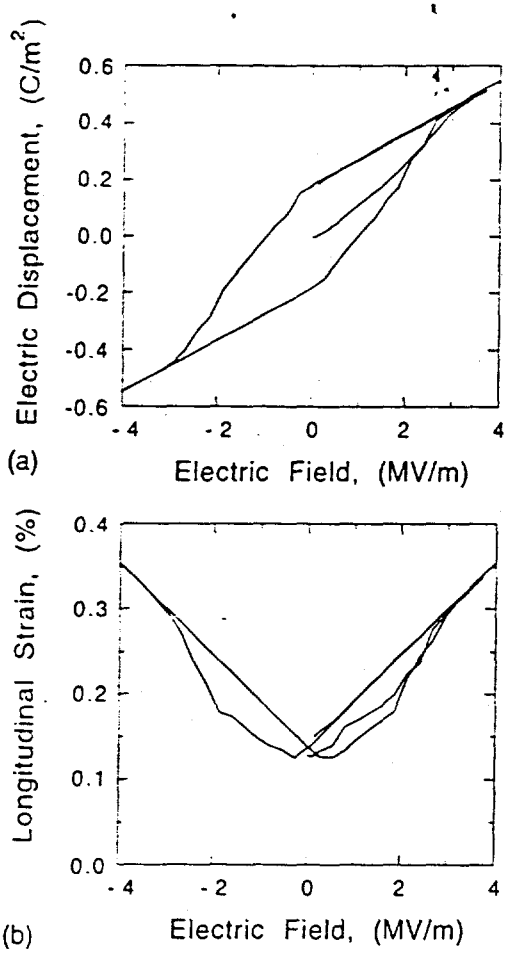

FIG. 4. Simulated 8/65/35 PLZT hysteresis loops with the critical field for 90° switching E_o^{90} = 0.1 MV/m and the critical field for 180° switching E_o^{180} = 1.0 MV/m. (a) Electric displacement *versus* electric field. (b) Axial strain *versus* electric field.

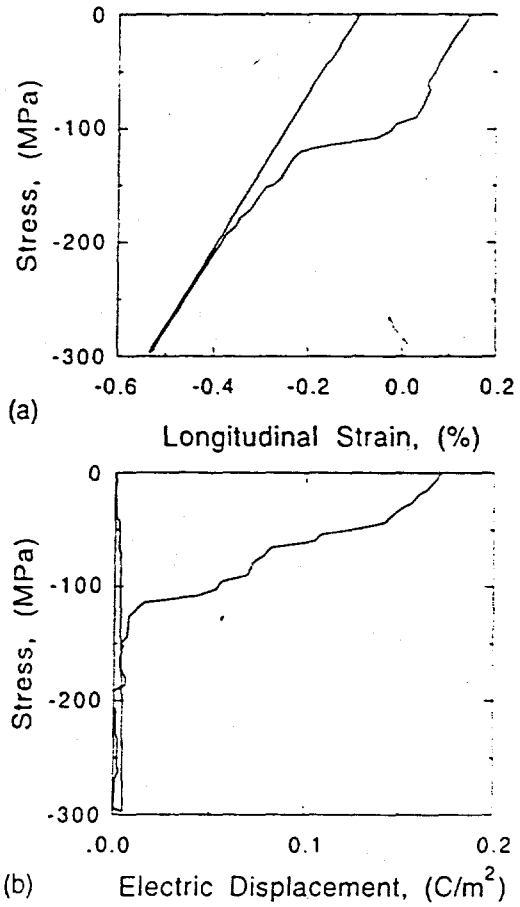

FIG. 5. Simulated 8/65/35 PLZT stress *versus* strain and stress *versus* electric displacement curves for a poled ceramic with the critical field for 90° switching E_o^{90} = 0.1 MV/m and the critical field for 180° switching E_o^{180} = 1.0 MV/m. (a) Axial stress *versus* axial strain. (b) Axial stress *versus* electric displacement.

7. DISCUSSION

The model developed in this paper has 8 disposable parameters. Among the parameters, Young's modulus Y, Poisson's ratio υ, dielectric permittivity ε, and piezoelectric coefficient d_{333} are the experimentally measured values[19]; the magnitude of the spontaneous strain e_0 is required to match the remanent strain and the spontaneous polarization P_0 is required to match the remanent polarization of the experimental data of a PLZT ceramic. The other parameters are the effective critical field for 90° switching E_o^{90} and the critical field for 180° switching E_o^{180}[26] and are available for adjustment.

Regardless of the chosen effective critical fields, none of the simulations presented in this article successfully predicts the measured hysteresis loops of PLZT[19]. Although true ferroelectric switching occurs by domain wall motion[2-4,22,48], the finite element model neglects the details of the wall motion. Instead, the model is based upon potential energy and the balance of work during switching; it treats switching in crystallites as an abrupt phenomenon controlled by the applied mechanical or electrical load constrained by nearest neighbor interactions and by macroscopic elastic, dielectric and piezoelectric energy; thus, the finite element model is more closely related to the Landau-Ginzburg-Devonshire model (i.e. a double-well potential model for unit cell switching)[27,29,30] than to the Avrami model (i.e. a nucleation and growth model for switching in a single crystal or polycrystalline ceramic)[31-34]. In the case of the finite element model, there are multiple energy wells corresponding to each possible combination of polarization in the finite element. Note that the effective fields of switching, E_o^{90} and E_o^{180}, fitted parameters in the finite element model, are of the same order of magnitude as the measured coercive field, whereas the Landau-Ginzburg-Devonshire model predicts a coercive field one or two orders of magnitude larger than that the measured value[2].

In addition, the presented model neglects the spatial fluctuations of electric and stress fields within an element representing a crystallite. The model simply assumes that complete switching takes place in a crystallite when it meets the critical condition for repolarization evaluated at the centroid of the finite element. Thus, our switching criterion in eq. (42) involves interaction energies that are too large. Consequently, switching occurs locally without propagating through the ceramic because the crystallites do not yield either mechanically and electrically due to the resistance generated by the interaction energy terms in the criterion. The simulation will reproduce the experimental data (e.g. the tails of the butterfly loop) if and only if many neighbors of a switched crystallite undergo follow-up switching[41,43]. Such a simulation could be carried out by an improved version of the finite element method. For example, a model which includes the phenomenon of domain wall motion can be developed by implementing a laminar structure of 90° domains[44,45]. The domain structure with a more gradual strain change upon transformation than that occuring in the complete switching of a crystallite is expected to improve the predicting capability of the model.

ACKNOWLEDGMENTS

One of the authors (S.C.H.) is grateful for financial support by Prof. R. Waser of Forschungszentrum Jülich with its visiting scientist fellowship; this author is also indebted to Prof. G. Arlt of Aachen University of Technology for many helpful discussions. The work of R.M.M. was supported by National Science Foundation Grant 9813022.

REFERENCES

1. Little, A.L., "Dynamic Behavior of Domain Walls in Barium Titanate," *Phys. Rev.*, 98, 978, 1955.
2. Jona, F. and G. Shirane, *Ferroelectric Crystals*, Pergamon Press, New York, 1962.
3. Fatuzzo, E. and W.J. Merz, *Ferroelectricity*, North-Holland, Amsterdam, 1967.
4. W.F. Deeg, "The Analysis of Dislocation, Crack and Inclusion Problems in Piezoelectric Solids," Ph.D. Dissertation, Stanford University, 1980.
5. Cross, L.E. and R.E. Newnham, "History of Ferroelectrics," in *The Ceramics and Civilization*, Vol. III, *High Technology Ceramics-Past, Present, and Future*, p. 289, Eds. W.D. Kingery and E. Lense, American Ceramic Society, Westerville, OH., 1986.
6. Haertling, G.H., "PLZT Electroptic Materials and Applications-A Review," *Ferroelectrics*, 75, 22, 1987.
7. Scott, J.F. and C.A. Paz de Araujo, "Ferroelectric Memories," *Science*, 246, 1400, 1989.
8. Polla, D.L., and L.F. Francis, "Ferroelectric Thin Films in Micro-electromechanical Systems Applications," *MRS Bulletin*, 21[7], 59, 1996.

9. Randall, C.A., N. Kim, J.P. Kucera, W. Cao, and T.R. Shrout, "Intrinsic and Extrinsic Size Effects in Fine-Grained Morphotropic-Phase-Boundary Lead Zironate Titanate Ceramics," *J. Am. Ceram. Soc.*, 81, 677, 1998.
10. Tanaka, M. and Y. Makino, "Finite Size Effects in Submicron Barium Titanate Particles," *Ferroelectric Lett. Sect.*, 24, 13, 1998
11. McCauley, D., R.E. Newnham, and C.A. Randall, "Intrinsic Size Effects in a Barium Titanate Glass-Ceramics," *J. Am. Ceram. Soc.*, 81, 979, 1998.
12. Ahn, C.H., T. Tybell, L. Antognazza, K. Char, R.H. Hammond, M.R. Beasley, O. Fischer, J.-M. Triscone, "Local, Nonvolatile Electronic Writing of Epitaxial $Pb(Zr_{0.52}Ti_{0.48})O_3/SrRuO_3$ Heterostructures," *Science*, 276, 1100, 1997.
13. Hidaka, T., T. Maruyama, M. Saitoh, N. Mikoshiba, M. Shimizu, T. Shiosaki, L.A. Wills, R. Hiskes, S.A. Dicarolis, and J. Amano, "Formation and Observation of 50nm Polarized Domains in $PbZr_{1-x}Ti_xO_3$ Thin Film Using Scanning Probe Microscope," *Appl. Phys. Lett.*, 68, 2358, 1996.
14. Gruverman, A., H. Tokumoto, A.S. Prakash, S. Aggarwal, B. Yang, M. Wuttig, R. Ramesh, O. Auciello, and T. Venkatesan, "Nanoscale Imaging of Domain Dynamics and Retention in Ferroelectric Thin Films," *Appl. Phys. Lett.*, 71, 3492, 1997
15. Franke, K., H. Huelz, and M. Weihnacht, "Stress-induced Depolarization in PZT Thin Films, Measured by Means of Electric Force Microscopy," *Surf. Sci.*, 416, 59, 1998.
16. Damjanovic, D., "Stress and Frequency Dependence of the Direct Piezoelectric Effect in Ferroelectric Ceramics," *J. Appl. Phys.*, 82, 1788, 1997.
17. Mueller, V. and Q.M. Zhang,, "Shear Response of Lead Zirconate Titanate Piezoceramics," *J. Appl. Phys.*, 83, 3754, 1998.
18. Chan, K.H. and N.W. Hagood, "Modeling of Nonlinear Piezoceramics for Structural Actuation," *Proc. SPIE, Smart Struct. Mat.*, Ed. N.W. Hagood, 2190, 194, 1994.
19. Hwang, S.C., C.S. Lynch, and R.M. McMeeking, "Ferroelectric Ferroelastic Interactions and a Polarization Switching Model," *Acta metall. mater.*, 43, 2073, 1995.
20. Wang, Y., S-X. Gong, H. Jiang, and Q. Jiang, "Modeling of Domain Pinning Effect in Polycrystalline Ferroelectric Ceramics," *Ferroelectrics*, 182, 62, 1996.
21. Chen, X., D.N. Fang, and K.C. Hwang, "Micromechanics Simulation of Ferroelectric Polarization Switching," *Acta mater.*, 45, 3181, 1997.
22. Hwang, S.C., *Polarization Switching Models in Polycrystalline Ferroelectric Ceramics*, Ph. D. Thesis, University of California, Santa Barbara, 1997
23. Hwang, S.C., J.E. Huber, R.M. McMeeking, and N.A. Fleck, "The Simulation of Switching in Polycrystalline Ferroelectric Ceramics," *J. Appl. Phys.*, 84, 1530, 1998.
24. Hwang S.C. and R.M. McMeeking, "A Finite Element Model of Ferroelectric Polycrystals", *Ferroelectrics*, 211, 177, 1998.
25. Hwang S.C. and R.M. McMeeking, "A Finite Element Model of Ferroelastic Polycrystals", *Int. J. Solids Struct.*, 36, 1541, 1999.
26. Huber, J.E., N.A. Fleck, C.M. Landis, and R.M. McMeeking, "A Constitutive Law for Ferroelectric Polycrystals," *J. Mech. Phys. Solids*, 47, 1663, 1999.
27. Jaffe, B., W.R. Cook and H. Jaffe, *Piezoelectric Ceramics*, Academic Press, London and New York, 1971.
28. Cady, W.G., *Piezoelectricity*, Vols. 1 & 2, Dover, New York, 1964.
29. Devonshire, A.F., "Theory of Barium Titanate.-Part I," *Phil. Mag.*, 40, 1040, 1949.
30. Landau, L.D. and E.M. Lifshitz, *Electrodynamics of Continuous Media*, Pergamon Press, New York, 1960.
31. Avrami, M. "Kinetics of Phase Change I: General Theory," *J. Chem. Phys.*, 7, 1103, 1939.
32. Avrami, M. "Kinetics of Phase Change II: Transformation-Time Relations for Random Distribution of Nuclei," *J. Chem. Phys.*, 8, 212, 1940.
33. Avrami, M. "Kinetics of Phase Change III: Granulation, Phase Change, and Microstructure," *J. Chem. Phys.*, 9, 177, 1941.
34. Ishibashi, Y. and Y. Takagi, "Note on Ferroelectric Domain Switching," *J. Phys. Soc. Jpn.*, 31, 506, 1971.
35. Randall, C.A., D.J. Barber, and R.W. Whatmore, "Ferroelectric Domain Configurations in a Modified-PZT Ceramic," *J. Mater. Sci.*, 22, 925, 1987.
36. Stratton, J.A., *Electromagnetic Theory*, McGraw-Hill, London, 1941.
37. Maugin, G.A., *Continuum Mechanics of Electromagnetic Solids*, North-Holland, Amsterdam, 1988.
38. Allik, H. and T.J.R. Hughes, "Finite Element Method for Piezoelectric Vibration," *Int. J. Numer. Meth. Eng.*, 2, 151, 1970.

39. Cook, R.D., D.S. Malkus, and M.E. Plesha, *Concepts and Applications of Finite Element Analysis*, John Wiley & Sons, New York, 1989.
40. Press, W.H., S.A. Teukolsky, W.T. Vetterling, and B.P. Flannery, *Numerical Recipes in C: the Art of Scientific Computing*, 2nd ed., Cambridge University Press, New York, 1992.
41. Hwang, S.C. and R. Waser, "Study of Electrical and Mechanical Contribution to Switching in Ferroelectric/Ferroelastic Polycrystals," submitted to *Acta mater.*, 2000.
42. Lord Rayleigh, "On the Behavior of Iron and Steel under the Operation of Feeble Magnetic Forces," *Phil. Mag.*, 23, 225, 1887.
43. Hwang, S.C. and G. Arlt, "Switching in Ferroelectric Polycrystals," *J. Appl. Phys.*, 87, 869, 2000.
44. Arlt, G., "Switching and Dielectric Nonlinearity of Ferroelectric Ceramics," *Ferroelectrics*, 189, 91, 1996.
45. Kovalev, S. and M. Sakai, "Numerical Modeling of Electro-Elastic Field in Ferroelectric Crystal Containing 90° Twin Boundary," *Acta mater.*, 46, 3015, 1998.

(Submitted to *Proceedings to SPIE: Smart Structures and Materials*)

February, 2000